Direct evidence of quantum transport in photosynthetic light-harvesting complexes

Gitt Panitchayangkoon[a,1], Dmitri V. Voronine[b,1], Darius Abramavicius[c,d], Justin R. Caram[a], Nicholas H. C. Lewis[a], Shaul Mukamel[e], and Gregory S. Engel[a,2]

[a]Department of Chemistry and The James Franck Institute, The University of Chicago, Chicago, IL 60637; [b]Institute for Quantum Science and Engineering, Department of Physics and Astronomy, Texas A&M University, College Station, TX 77843; [c]Physics Faculty, Vilnius University, LT-10222, Vilnius, Lithuania; [d]State Key Laboratory of Supramolecular Structure and Materials, Jilin University, Changchun 130012, People's Republic of China; and [e]Department of Chemistry, University of California, Irvine, CA 92697

Edited by* Peter M. Rentzepis, University of California, Irvine, CA, and approved October 17, 2011 (received for review April 04, 2011)

The photosynthetic light-harvesting apparatus moves energy from absorbed photons to the reaction center with remarkable quantum efficiency. Recently, long-lived quantum coherence has been proposed to influence efficiency and robustness of photosynthetic energy transfer in light-harvesting antennae. The quantum aspect of these dynamics has generated great interest both because of the possibility for efficient long-range energy transfer and because biology is typically considered to operate entirely in the classical regime. Yet, experiments to date show only that coherence persists long enough that it can influence dynamics, but they have not directly shown that coherence does influence energy transfer. Here, we provide experimental evidence that interaction between the bacteriochlorophyll chromophores and the protein environment surrounding them not only prolongs quantum coherence, but also spawns reversible, oscillatory energy transfer among excited states. Using two-dimensional electronic spectroscopy, we observe oscillatory excited-state populations demonstrating that quantum transport of energy occurs in biological systems. The observed population oscillation suggests that these light-harvesting antennae trade energy reversibly between the protein and the chromophores. Resolving design principles evident in this biological antenna could provide inspiration for new solar energy applications.

energy transport | photosynthesis | quantum biology | ultrafast phenomena

Photosynthetic organisms employ light-harvesting antennae to capture and transport solar energy to the reaction center where charge separation occurs. This energy transport process proceeds through a complex network of coupled chromophores embedded in protein matrices of light-harvesting antenna complexes. Because of static Coulombic dipole couplings, the excitation typically delocalizes among two or more chromophores—these delocalized excited states are known as "excitons." Though the excitonic states only delocalize across the chromophores, the protein bath is necessary for enabling energy transport by allowing the system to dissipate energy.

The precise mechanism of dissipation and whether the protein helps to steer the transport remain interesting and open questions regarding optimal design of energy transport in disordered systems. In most electronic systems, coherences among states dephase far faster than the states themselves can relax thereby precluding contributions of coherence to relaxation processes. We define transport in such systems as "classical." Microscopically, classical transport arises from small, independent fluctuations within the protein that enable relaxation of excitonic populations through resonance energy transfer (1–4). This incoherent mechanism gives rise to exponential relaxation dynamics and ignores coherent dynamics.

Recent studies on photosynthetic complexes reveal that quantum coherence persists on the same timescale as population transfer—long enough to impact transport dynamics (5–9). This experimental data implies that quantum coherences should not be ignored in photosynthetic antenna systems. Long-lived quantum coherence alone, however, is not sufficient to produce high quantum efficiency. For quantum coherences to affect efficiency or biological function, the coherences must drive dynamics and change the probability of finding the excitation in a given state. That is, coherences must couple to populations. We denote this regime as "quantum transport."

In this study, we revisit two-dimensional electronic spectra of photosynthetic systems published previously to seek evidence of coupling between quantum coherences and excited-state populations that provide direct signatures of quantum transport (9). These data show long-lived quantum coherence in the Fenna–Matthews–Olson (FMO) complex of the green sulfur bacteria, *Chlorobaculum tepidum*. This phenomenon has been the subject of many studies, both theoretical and experimental (10–12). Such long-lived coherence could potentially lead to quantum transport.

Recent theoretical work has identified oscillatory probability distributions as the signature of quantum transport (13). Conclusively identifying the origin of an oscillatory signal as arising from either population or coherence dynamics, however, presents an experimental challenge. To help discern population oscillation signals from those of quantum coherence, we start by examining transport dynamics using Redfield master equation. We show that the population oscillations appear in our data and they can be linked to quantum transport through a unique phase relationship. We conclude by discussing the implications of quantum transport both for our understanding of the microscopic protein environment and our phenomenological understanding of energy transfer.

To derive the origin of the oscillating probabilities, we represent the excitonic states of the FMO complex statistically as a quantum ensemble using the reduced density operator formalism (14). We expand the density operator, ρ, in the excitonic basis, $|e_n\rangle$, which are time-independent eigenstates constructed from linear combinations of the coupled excited states of the bacteriochlorophyll *a* chromophores (the sites). This excitonic basis corresponds to the eigenbasis of the time-averaged system Hamiltonian, and we will restrict our discussion throughout this paper to this basis. In this representation, the reduced density matrix is

$$\hat{\rho} = \sum_{i,j} \langle c_i(t) c_j^*(t) \rangle |e_i\rangle\langle e_j| = \sum_{i,j} \rho_{ij} |e_i\rangle\langle e_j|. \quad [1]$$

The diagonal elements of the density matrix, $\rho_{ii} = \langle c_i c_i^* \rangle$, represent ensemble populations. The off-diagonal elements, ρ_{ij} for

Author contributions: G.P., D.V.V., D.A., S.M., and G.S.E. designed research; G.P. D.V.V., D.A., S.M., and G.S.E. performed research; G.P., D.V.V., D.A., J.R.C., N.H.C.L., S.M., and G.S.E. analyzed data; and G.P., D.V.V., D.A., S.M., and G.S.E. wrote the paper.

The authors declare no conflict of interest.

*This Direct Submission article had a prearranged editor.

[1]G.P and D.V.V. contributed equally to this work.

[2]To whom correspondence should be addressed. E-mail: gsengel@uchicago.edu.

This article contains supporting information online at www.pnas.org/lookup/suppl/doi:10.1073/pnas.1105234108/-/DCSupplemental.

$i \neq j$, represent coherences and are complex numbers carrying phase information. Experimentally, we probe the ensemble average of the populations or coherences over bath realizations.

Quantum dynamics within photosynthetic complexes are typically modeled with second-order perturbation theory using Lindblad or Redfield master equations. Although each method has different strengths and weaknesses (and both reproduce the dynamics discussed here), we choose to use the Redfield master equation for this work because it conveniently separates unitary time evolution from dissipative dynamics and clearly illustrates the origin of quantum transport due to coupling between populations and coherences. The Redfield master equation can be expressed as

$$\frac{\partial \hat{\rho}}{\partial t} = -\frac{i}{\hbar}[\hat{H},\hat{\rho}] - \hat{\kappa}\,\hat{\rho}\,, \qquad [2]$$

where $\hat{H}$ is the system Hamiltonian, and $\hat{\kappa}$ is the relaxation superoperator. In essence, all the dynamics important for function are contained within the relaxation superoperator. Treating the interaction perturbatively, an expansion of the Redfield equation for the system of excitonic states yields

$$\frac{\partial \rho_{ij}}{\partial t} = -\frac{i}{\hbar}(\varepsilon_i - \varepsilon_j)\rho_{ij} - \sum_{kl}\kappa_{ij,kl}\rho_{kl}. \qquad [3]$$

The Redfield equation shows that temporal evolution of a particular element of the density matrix depends on the energy of the system eigenstates, ε_n, as well as on relaxation within the system. The relaxation dynamics are captured within the relaxation superoperator, $\hat{\kappa}$; elements $\kappa_{ij,kl}$ determine how element ρ_{kl} will contribute to the time evolution of the element ρ_{ij} of the density matrix. The physical origin of the relaxation superoperator arises from fluctuations from the time-averaged Hamiltonian that instantaneously affect the eigenstates by effectively mixing them. The relaxation superoperator elements can be divided into three different classes: population transfer terms, $\rho_{kk} \rightarrow \rho_{ii}$ ($\kappa_{ii,kk}$), representing classical transport; coherence transfer terms, $\rho_{kl} \rightarrow \rho_{ij}$ for $k \neq l$ and $i \neq j$ ($\kappa_{ij,kl}$); and coupling between populations and coherences, $\rho_{kl} \rightarrow \rho_{ii}$ for $k \neq l$ ($\kappa_{ii,kl}$). The $\kappa_{ii,kl}$ terms represent quantum transport by our definition.

Simply interpreted, the Redfield equation represents a first-order differential rate law that describes the change in each element in the density matrix. Two different processes control the rate of change of ρ_{ij}: unitary dynamics, $-\frac{i}{\hbar}(\varepsilon_i - \varepsilon_j)\rho_{ij}$, and nonunitary contributions (relaxation) due to coupling to other elements of the density matrix, $\sum_{kl}\kappa_{ij,kl}\rho_{kl}$. Unitary dynamics is responsible for the sinusoidal phase oscillation of coherences. As a result, we observe quantum coherence as an oscillation in peak amplitude, or quantum beat, with a fixed frequency proportional to the energy gap. For a population term, however, the rate of change depends only on relaxation dynamics because the unitary oscillation vanishes when the energy gap $\varepsilon_i - \varepsilon_j$ is zero. For a population term, the summation notation expands to

$$\frac{\partial \rho_{ii}}{\partial t} = -\sum_{kl}\kappa_{ii,kl} = \underbrace{-\sum_{k}(\kappa_{ii,kk}\rho_{kk} - \kappa_{kk,ii}\rho_{ii})}_{\text{Resonance Energy Transport}} - \underbrace{\sum_{k\neq l}\kappa_{ii,kl}\rho_{kl}}_{\text{Quantum Transport}}. \qquad [4]$$

From Eq. **4**, we can see that population dynamics is governed by two distinct mechanisms: The first term represents transfer to and from other populations via resonance energy transport, and the second term causes oscillations driven by coherences. Population transfer via incoherent, resonance energy transport leads to exponential growth or decay depending on the direction of transport. The final term in Eq. **4** shows that populations will take on the oscillatory character of coherences.

Fig. 1 schematically depicts the three types of transfer possible among elements of the density matrix. In classical resonance energy transfer (blue), the dynamics is mostly confined to the electronic states of the chromophores. That is, energy is transferred monotonically from one state to the next, and the population dynamics is entirely decoupled from the coherence dynamics. Next, coherence transfer (green) can accompany the population transfer allowing relaxation from one superposition state to another. In quantum transport (red), coherences and populations couple, allowing coherences to drive transfer between populations. This process yields oscillatory population dynamics.

Results

To search for evidence of quantum transport in photosynthetic systems, we revisit two-dimensional electronic spectroscopic data on the FMO complex published previously (9). (A complete discussion of methods and materials can be found in ref. 9.) Phase-sensitive two-dimensional electronic spectroscopy permits observation and characterization of population and coherence dynamics (15). The experimental and theoretical details for this spectroscopy have been described elsewhere (16–19). In essence, the data from 2D spectroscopy can be interpreted as a correlation map (ω_τ,ω_t) of the "input" energy, $\hbar\omega_\tau$, and the "output" energy, $\hbar\omega_t$. A series of 2D spectra as a function of waiting time reveals time-dependent evolution of a system after excitation. In rephasing pathways, the photon echo eliminates inhomogeneous broadening in the antidiagonal direction, which further improves spectral resolution. The diagonal peak ($\omega_\tau = \omega_t$) contains information on the population states and their relaxation dynamics. The existence of a cross-peak ($\omega_\tau \neq \omega_t$) indicates a coupling and transfer pathway between population states that cannot be observed directly using linear absorption spectroscopy. The spectral positions of the cross-peaks help to identify couplings and coherences between excitonic states. Theoretical studies predict quantum beating due to unitary evolution of coherences will appear in cross-peaks in rephasing pathways but not in diagonal peaks (20).

We start our investigation by first isolating the coherence beating signal due to unitary evolution using the same procedure discussed in detail in prior works (9, 21). This coherence beating signal is used only for comparison to determine whether coher-

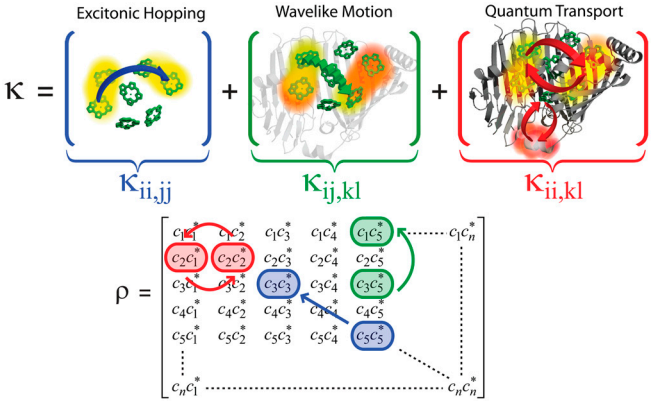

Fig. 1. The Redfield relaxation superoperator contains three types of transfer elements: transfer between populations (blue), transfer between coherences (green), and transfer between a population and a coherence (red). These transfer mechanisms are depicted schematically both in the FMO photosynthetic antenna complex and in the density matrix. Quantum transport (red) occurs when populations and coherences directly couple. Each transfer scheme implies a different type of interaction with the protein environment, with the most active contribution occurring in the quantum transport regime.

CHEMISTRY

ences couple to populations. A representative absorptive rephasing 2D spectrum of the FMO complex is shown in Fig. 2 (*Inset*). We consider only the absorptive (real) portion of the rephasing signal, which eliminates contributions from interfering response pathways and improves spectral resolution. On the diagonal, excitonic features blend together, but the lowest energy exciton 1 peak is most well resolved. Downhill energy transfer between two coupled excitonic states gives rise to cross-peaks below the diagonal. Because of peak broadening and the small energy difference between excitons 2 and 3, the cross-peaks between excitons 1 and 2 and between excitons 1 and 3 overlap with each other, apparently forming one well-resolved cross-peak below the main diagonal.

We observe two pronounced quantum beating frequencies within the amplitude oscillations of the most well-resolved cross-peak (green dot) (21). The coherence beating signal (green trace) in Fig. 2 was obtained by subtracting two exponentials corresponding to population transfer dynamics. A Fourier transform of this signal reveals approximately twice as great a contribution from the lower frequency (ω_{12}) component as from the high frequency component (ω_{13}).

Next, we isolate the population signal. In rephasing 2D spectra, the perturbative pathways used to probe the populations all involve interactions with light of the same color. Therefore, signals associated with populations will appear on the main diagonal ($\omega_\tau = \omega_t$). We hypothesize that coupling between populations and coherences will be strongest for coherence and populations involving a common state. Therefore, we expect the coherence signal isolated above to drive population oscillations on the main diagonal features either directly above or directly to the left of the observed coherence signal. The width of our laser spectrum precludes precise measurements of the lowest energy exciton population. We therefore extrapolate vertically from the cross-peak signal to the main diagonal to extract a population signal.

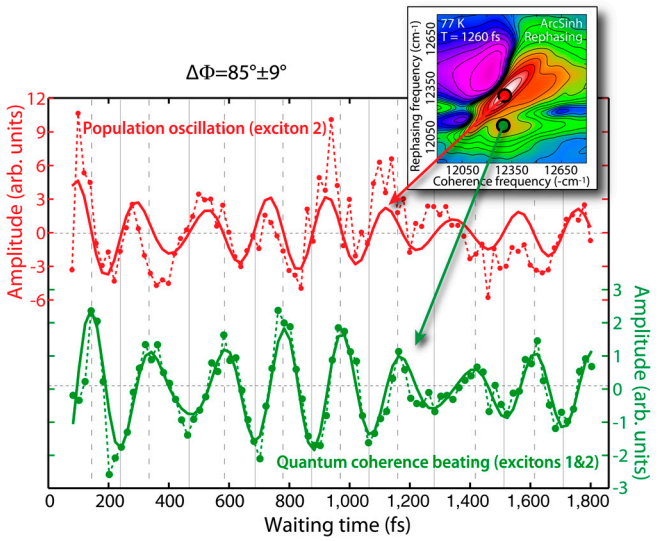

Fig. 2. An overlay of quantum coherence beating (green) and population oscillation (red) highlights the 90° phase shift in the experimental signals extracted from rephasing data. This observed phase shift results from a coupling between the oscillating coherence signal to the time-derivative of population dynamics. The experimental data are shown in solid circles connected by dashed lines, and the fits are shown in solid lines. A representative 2D spectrum from a rephasing pathway at $T = 1{,}260$ fs is shown in the *Inset*; the green and red circles highlight the spectral position from which the signals are extracted. The fit of the population oscillation signal is obtained by adjusting only the phase and amplitudes of the fit of the coherence signal. Although the model successfully captures the frequency and position of the extrema, the population signal also couples to other coherences giving rise to fluctuations not captured by this model.

As we will show later, the observed signal appears throughout the lower part of the diagonal feature and is not strongly dependent on this choice.

To isolate the oscillatory component of the population signal from the exponential relaxation dynamics, we again remove a biexponential decay. The data prior to $T = 80$ fs have been excluded from our analysis to avoid pulse overlap effects. The resulting oscillatory population signal (red) is plotted in Fig. 2 above the quantum coherence beating signal (green) described previously. We observe pronounced oscillation in the population with similar frequencies to those in the coherence signal but phase-shifted from the coherence signal. As a control, we have checked that this result does not change qualitatively if the initial coherence time points are discarded providing discrimination against pulse overlap in the indirect, τ, domain as well.

We examine this phase shift further by quantifying the frequency and phase of the population signal relative to the quantum coherence beating. Using the procedure described by Hayes et al. (21), we first fit the cross-peak quantum beating signal with a linear combination of two exponentially damped sine functions,

$$S_{\mathrm{coh}}(T) = A_{12}\sin(\omega_{12}T + \phi_{12})e^{-\gamma_{12}T} + A_{13}\sin(\omega_{13}T + \phi_{13})e^{-\gamma_{13}T}, \quad [5]$$

where $A_{12(13)}$, $\omega_{12(13)}$, $\phi_{12(13)}$, and $\gamma_{12(13)}$ represent the magnitude, frequency, phase, and lifetime associated with the coherence signal from excitons 1 and 2 (1 and 3) (all regression parameters are given in Supporting Information). Next, we model the functional form of the population oscillation signal. For this regression, we hold $A_{12(13)}$, $\omega_{12(13)}$, $\phi_{12(13)}$, and $\gamma_{12(13)}$ constant based on the above fit to the coherence signal and fit only three parameters: a phase shift, $\Delta\Phi$, and two weighted contributions, $\kappa_{22,12}$ and $\kappa_{22,13}$, representing the relaxation superoperator elements that link coherences to population,

$$S_{\mathrm{coh}\to\mathrm{pop}}(T) = \kappa_{22,12}A_{12}\sin(\omega_{12}T + \phi_{12} + \Delta\Phi)e^{-\gamma_{12}T} + \kappa_{22,13}A_{13}\sin(\omega_{13}T + \phi_{13} + \Delta\Phi)e^{-\gamma_{13}T}. \quad [6]$$

A comparison of the fits (solid) and raw data (dashed) is shown in Fig. 2. The resultant phase shift is approximately 90° ($\Delta\Phi = 85 \pm 9°$). The 90° phase shift of the population oscillation signal allows us to exclude the possibility that this signal is quantum beating due to unitary evolution of the coherences. This phase shift also effectively discriminates against signals arising from the wings of the coherence feature; such a signal would be in phase with the coherence signal. Similarly, coherence beating due to an excited-state absorption pathway would be 180° out of phase.

This 90° phase shift is unusual in two-dimensional spectroscopy. We designed a filter to better visualize the extent of this signal. We employ a z-transform filter because it maintains phase information while providing better filtering than a simple Fourier transform (22). Applying a z-transform filter across the waiting time, T, axis of the dataset, we isolate long-lived beating signals (dephasing rate, Γ, less than 30 cm^{-1}) with a beat frequency, ω_T, between 155 and 163 cm^{-1}, corresponding to the difference frequency between excitons 1 and 2 (23). This beating signal appears in our data only at the position of the expected exciton 1-2 cross-peak and on the diagonal directly above it (Fig. 3*A*). The phase of the signal (Fig. 3*B*) shows the characteristic phase shift of approximately 90° throughout the spectral feature. A similar relationship exists for the 200 cm^{-1} beat frequency corresponding to the difference frequency between excitons 1 and 3 (see Supporting Information). This filter confirms that the signal is specific to the exciton and population in question and does not arise from vibration, laser fluctuations, or other noise sources.

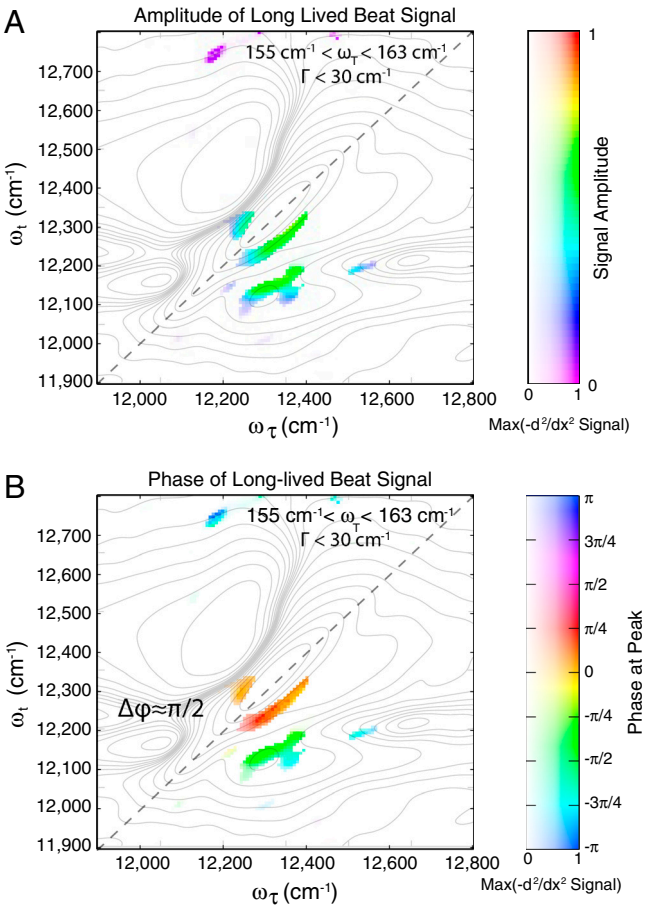

Fig. 3. Two-dimensional data filtered in the waiting time, T, domain using a z-transform to select long-lived beating signals (dephasing rate, Γ, less than 30 cm^{-1}) with a beat frequency, ω_T, between 155 and 163 cm^{-1} corresponding to the energy difference between excitons 1 and 2. For each point in the spectrum, the saturation (whiteness) is determined by whether the data shows a long-lived beating signal of the appropriate frequency, whereas the hue is determined by the amplitude (*A*) or phase (*B*) of the beating signal. The colored regions show that the beating signal appears only on the cross-peak and associated diagonal peak, suggesting electronic quantum coherence as the origin of the signal. In contrast, an oscillatory signal due to vibrational coherence or power fluctuations would appear throughout the spectrum. The 90° phase difference between the coherence (off-diagonal) and population (diagonal) signals is a signature of quantum transport. Contour lines from the $T = 1{,}260$ fs spectra from Fig. 2 are included in light gray for reference.

Discussion

Oscillations occur in both the coherence beating signal and in the population signal shown in Fig. 2. The existence and position of the coherence beating signal agree well with a theoretical study by Cheng and Fleming (20). However, electronic quantum coherence cannot explain beating on the diagonal in the rephasing pathway. Quantum transport simultaneously explains the oscillation observed on the diagonal signal and the observed phase relationship.

To understand this 90° phase shift, we again examine the relationship between coherences and populations created by quantum transport terms derived in Eq. **4**. The quantum transport term demonstrates that the time derivative of population will include an oscillatory component due to coupling to coherences. Just as the integral of cosine is sine, the Redfield equation predicts that population oscillations should have a 90° phase shift from the coherence terms that drive them. No other mechanism has been suggested to create a signal phase-shifted by 90°. We therefore interpret the observed population oscillation as evidence of quantum transport and verify coupling between populations and coherences.

Beyond the oscillations observed here, quantum transport has many ramifications that help explain other observations in photosynthetic complexes. For example, although the current analysis focuses on how coherences drive population oscillations, it is interesting to consider the opposite process through which populations couple to coherences allowing them to borrow lifetime from populations. This process directly explains observations of long-lived quantum coherence. In a more microscopic analogy, the population oscillations can be thought of as Rabi-like oscillations that indicate strong mixing between the excitonic system and the bath (as compared to a true Rabi oscillation arising from strong coupling to an optical field). Following this analogy to Rabi oscillations, we can speculate that the coupling between the system and bath is strong enough that fluctuations in the protein bath effectively entangle bath modes with the system in a nontrivial way. This entangling allows the excitonic states of the FMO to trade energy with the protein bath on a femtosecond timescale.

The observed coupled dynamics of populations and coherences demonstrates a unique and more active role of the protein matrix in energy transport beyond the coherence protection mechanisms proposed by Lee et al., which invoked weakly coupled correlated baths (6). Furthermore, an oscillation in probability distribution in the nondegenerate excitonic states suggests that the total energy of the "system" may not be conserved. An oscillation in total energy of the chromophores does not impugn energy conservation, but again suggests that the system is strongly coupled to the bath such that a varying amount of the excitation is delocalized onto the bath modes as a function of time. We hypothesize that some energy is reversibly transferred between the chromophores and these bath modes throughout the transport process. To fully capture this time-dependent mixing of system and bath, we must consider the protein bath (or some portion of it) as an integral part of the energy transport system.

In summary, the oscillatory population dynamics that we observe suggests protein-assisted coupling between populations and coherences. As population feeds into coherences, coherence lifetime increases to match nonequilibrium population lifetime. In addition, transfer of coherence into population drives the population dynamics and imparts an oscillatory behavior to the energy transfer process. This observation provides direct evidence of quantum transport through the FMO complex. Because the excited states of the FMO complex are nondegenerate in energy, oscillating populations imply oscillations of the total excitonic energy. This dynamics requires that the system become mixed with the protein bath, leading to reversible exchange of energy between the two. Such a time-dependent mixing of system and bath demands a rethinking of the nature of electronic excitations and their dynamics in complex solvation environments.

Materials and Methods

Sample Preparation. Trimers of the FMO from *Chlorobaculum tepidum* (24) in a buffer of 800 mM tris/HCl (pH 8.0) were mixed 35:65 vol/vol in glycerol with 0.1% lauryldimethylamine oxide detergent and loaded into a 200-μm fused quartz cell (Starna). The optical density at 809 nm was 0.32. A cryostat (Oxford Instruments) was used to cool the sample to 77 K.

Data Acquisition. A self mode-locking Ti:Sapphire oscillator (Coherent, Micra) was used to seed a regenerative amplifier (Coherent, Legend Elite), which produced a 5.0-kHz pulse train of 38-fs pulses centered at 806 nm with a spectral bandwidth of 35 nm. The 10-Hz stability of the laser power during data acquisition ranged from 0.08% to 0.19%. Two pairs of phase-locked beams were generated by a diffractive optic (Holoeye). All beams were incident on identical optics except for one-degree fused silica wedges (Almaz Optics) on delay stages (Aerotech), which determined the time delays. Each delay was calibrated using spectral interferometry as described elsewhere (18, 25).

Neutral density filters with total optical density 3.1 at 809 nm attenuated the local oscillator beam. The total power incident on the sample was 4.8 nJ (1.6 nJ/pulse), which was focused to a spot size less than 70 μm. A 0.3-m spectrometer (Andor Shamrock) frequency-resolved the emitted signal and

local oscillator beam, which were captured on a $1{,}600 \times 5$ pixel region of a back-illuminated, thermoelectrically cooled CCD (Andor Newton). Scatter subtraction, Fourier windowing, and transformation to frequency-frequency space were performed as described previously (18).

Two-dimensional data were collected at waiting times (T) in 20-fs increments for all temperatures. At each waiting time, the coherence time was scanned from -500 to 500 fs in steps of 4 fs. A 2D spectrum at $T = 0$ fs was taken every 200 fs to monitor sample integrity. No degradation was observed after 100 continuous 2D data acquisitions.

ACKNOWLEDGMENTS. We acknowledge the experimental efforts of Kelly Fransted and Dugan Hayes in collecting this data. We also acknowledge Jianzhong Wen and Robert E. Blankenship for providing the FMO sample. G.S.E. and G.P. acknowledge support from the Air Force Office of Scientific Research (FA9550-09-1-0117), the Defense Advanced Research Projects Agency (Grants N66001-10-1-4060 and N66001-10-1-4022), and the Searle Foundation for support of this work. S.M. gratefully acknowledges the support of National Science Foundation Grant CHE-1058791, Defense Advanced Research Projects Agency Grant BAA-10-40 QUBE, and the Chemical Sciences, Geosciences and Biosciences Division, Office of Basic Energy Sciences, Office of Science, US Department of Energy.

1. Forster T (1946) Energiewanderung Und Fluoreszenz. (Energy Transfer and Fluorescence). *Naturwissenschaften* 33:166–175 (in German).
2. Redfield AG (1965) The theory of relaxation processes. *Advances in Magnetic Resonance*, ed JS Waugh (Academic, New York), Vol 1.
3. Zhang WM, Meier T, Chernyak V, Mukamel S (1998) Exciton-migration and three-pulse femtosecond optical spectroscopies of photosynthetic antenna complexes. *J Chem Phys* 108:7763–7774.
4. Yang MN, Fleming GR (2002) Influence of phonons on exciton transfer dynamics: Comparison of the Redfield, Forster, and modified Redfield equations. *Chem Phys* 275:355–372.
5. Engel GS, et al. (2007) Evidence for wavelike energy transfer through quantum coherence in photosynthetic systems. *Nature* 446:782–786.
6. Lee H, Cheng YC, Fleming GR (2007) Coherence dynamics in photosynthesis: Protein protection of excitonic coherence. *Science* 316:1462–1465.
7. Calhoun TR, et al. (2009) Quantum coherence enabled determination of the energy landscape in light-harvesting complex II. *J Phys Chem B* 113:16291–16295.
8. Collini E, et al. (2010) Coherently wired light-harvesting in photosynthetic marine algae at ambient temperature. *Nature* 463:644–647.
9. Panitchayangkoon G, et al. (2010) Long-lived quantum coherence in photosynthetic complexes at physiological temperature. *Proc Natl Acad Sci USA* 107:12766–12770.
10. Plenio MB, Huelga SF (2008) Dephasing-assisted transport: Quantum networks and biomolecules. *New J Phys* 10:113019.
11. Rebentrost P, Mohseni M, Kassal I, Lloyd S, Aspuru-Guzik A (2009) Environment-assisted quantum transport. *New J Phys* 11:033003.
12. Sarovar M, Ishizaki A, Fleming GR, Whaley KB (2010) Quantum entanglement in photosynthetic light-harvesting complexes. *Nat Phys* 6:462–467.
13. Abramavicius D, Mukamel S (2010) Quantum oscillatory exciton migration in photosynthetic reaction centers. *J Chem Phys* 133:064510.
14. Mukamel S (1995) *Principles of Nonlinear Optical Spectroscopy* (Oxford Univ Press, New York) p xviii.
15. Cheng YC, Engel GS, Fleming GR (2007) Elucidation of population and coherence dynamics using cross-peaks in two-dimensional electronic spectroscopy. *Chem Phys* 341:285–295.
16. Hybl JD, Ferro AA, Jonas DM (2001) Two-dimensional Fourier transform electronic spectroscopy. *J Chem Phys* 115:6606–6622.
17. Cowan ML, Ogilvie JP, Miller RJD (2004) Two-dimensional spectroscopy using diffractive optics based phased-locked photon echoes. *Chem Phys Lett* 386:184–189.
18. Brixner T, Mancal T, Stiopkin IV, Fleming GR (2004) Phase-stabilized two-dimensional electronic spectroscopy. *J Chem Phys* 121:4221–4236.
19. Abramavicius D, Voronine DV, Mukamel S (2008) Unravelling coherent dynamics and energy dissipation in photosynthetic complexes by 2D spectroscopy. *Biophys J* 94:3613–3619.
20. Cheng YC, Fleming GR (2008) Coherence quantum beats in two-dimensional electronic spectroscopy. *J Phys Chem A* 112:4254–4260.
21. Hayes D, et al. (2010) Dynamics of electronic dephasing in the Fenna-Matthews-Olson complex. *New J Phys* 12:065042.
22. Tang J, Norris JR (1986) Two-dimensional LPZ spectral analysis with improved resolution and sensitivity. *J Magn Reson* 69:180–186.
23. Caram JR, Engel GS (2011) Extracting dynamics of excitonic coherences in congested spectra of photosynthetic light harvesting antenna complexes. *Faraday Discuss* 153:93–104.
24. Camara-Artigas A, Blankenship RE, Allen JP (2003) The structure of the FMO protein from Chlorobium tepidum at 2.2 angstrom resolution. *Photosynth Res* 75:49–55.
25. Lepetit L, Cheriaux G, Joffre M (1995) Linear techniques of phase measurement by femtosecond spectral interferometry for applications in spectroscopy. *J Opt Soc Am B Opt Phys* 12:2467–2474.

Supporting Information

Panitchayangkoon et al. 10.1073/pnas.1105234108

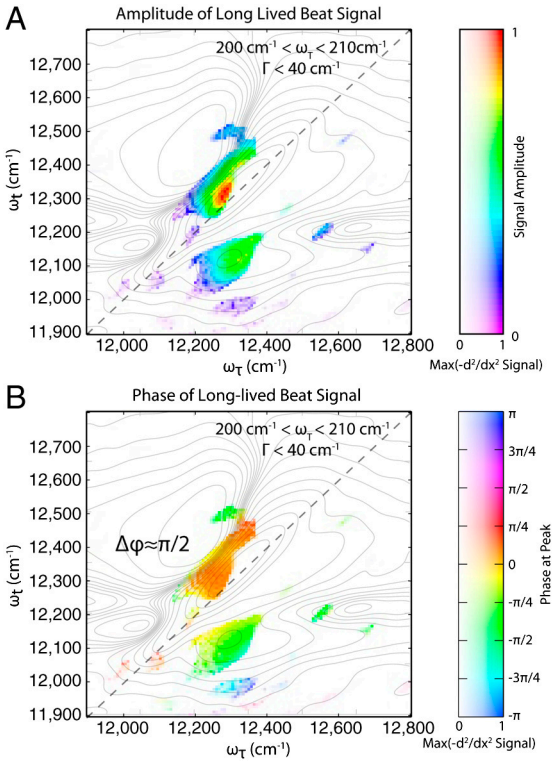

Fig. S1. Two-dimensional data filtered in the waiting time, T, domain using a linear prediction z-transform to select long-lived beating signals (dephasing rate, Γ, less than 40 cm^{-1}) with a beat frequency, ω_T, between 200 and 210 cm^{-1} corresponding to the energy difference between excitons 1 and 3. In order to generate this figure, a two-dimensional linear prediction z-transform was performed for each vector in (ω_τ ,ω_t T) using the method described by Tang and Norris (1). Linear prediction coefficients were determined in using the Yule–Walker equations that exist for autoregressive processes. This approach has been shown to work well for exponentially decaying sinusoids. For each point on the spectrum, the saturation (whiteness) is determined by the negative second derivative of the 2D linear prediction z-transform as determined by a Savitsky–Golay smoothing algorithm, whereas the hue is determined by the amplitude (A) or phase (B) of the beating signal. This isolates signals that are peaked in the selected region of interest in frequency-decay rate space. A similar pattern is observed to the data presented in Fig. 3, showing a 90° phase shift between diagonal and cross-peak signatures, suggesting that this is a common trait for other zero quantum coherences. Contour lines shown in light gray are taken from the $T = 1{,}260$ fs spectrum in Fig. 2 and included for reference.

1 Tang J, Norris JR (1986) Two-dimensional LPZ spectral analysis with improved resolution and sensitivity. *J Magn Reson* 69:180–186.

Table S1. The cross-peak signal is fit to two exponentially damped sine functions representing contribution from two coherences

A_{12}, arbitrary unit	1.90 ± 0.23
ω_{12}, cm^{-1}	161.3 ± 0.7
ϕ_{12}, °	185.8 ± 6.5
τ_{12}, fs	2,048.3 ± 559.5
A_{13}, arbitrary unit	1.00 ± 0.23
ω_{13}, cm^{-1}	198.7 ± 1.4
ϕ_{13}, °	187.9 ± 12.6
τ_{13}, fs	1,811.8 ± 877.0

$A_{12(13)}$ represents relative magnitude of coherence between excitons 1 and 2 (1 and 3). $\omega_{12(13)}$, $\phi_{12(13)}$, and $\gamma_{12(13)}$ are the frequency, phase, and lifetime associated with the coherence between excitons 1 and 2 (1 and 3). The uncertainty reported is 1 SD.

Table S2. The population oscillation signal is fit to the coherence beating signal by adjusting three parameters: a phase shift, $\Delta\Phi$, and two coupling constants, $\kappa_{22\leftarrow12}$ and $\kappa_{22\leftarrow13}$

$\Delta\Phi$, °	κ_{12}, arbitrary unit	κ_{13}, arbitrary unit
85.0 ± 9.1	1.94 ± 0.33	1.52 ± 0.65

The uncertainty reported is 1 SD.